Journal of Applied Geophysics xxx (2009) xxx–xxx

Contents lists available at ScienceDirect

Journal of Applied Geophysics

journal homepage: www.elsevier.com/locate/jappgeo

Evolution of post-seismic ground deformation of the Athens 1999 earthquake observed by SAR interferometry

M. Foumelis [a,*], Is. Parcharidis [b], E. Lagios [a], N. Voulgaris [a]

[a] National & Kapodistrian University of Athens, Faculty of Geology & Geoenvironment, Department of Geophysics — Geothermics, Panepistimiopolis, Ilissia, 157 84, Athens, Greece
[b] Harokopio University of Athens, Department of Geography, El. Venizelou 70, Kallithea, 176 71, Athens, Greece

ARTICLE INFO

Article history:
Received 21 April 2008
Accepted 8 February 2009
Available online xxxx

Keywords:
Differential interferometry
Post-seismic deformation
Athens earthquake

ABSTRACT

Co-seismic interferometric analysis was performed to investigate the spatial and temporal evolution of ground deformation related to the aftershock sequence of the Athens 1999 earthquake (M_w=6.0). Differential interferograms (DInSAR) spanning different periods after the main seismic event showed variable ground deformation associated with the evolution of the post-seismic displacement field. Using ERS SAR images, four co-seismic differential interferograms were generated for the period from September to December of 1999, and spanning 16, 32, 67 and 102 days after the occurrence of the main shock. It was found that the cumulative ground deformation detected by DInSAR analysis was exponentially decreasing, following the declining rate of the post-seismic activity. The observed propagation of the ground deformation maxima towards the SE direction is consistent with the presence of clustered aftershock activity to the east of the epicentral area. The aforementioned evolution of deformation was also recognized by the observed expansion of the displacement field to the east.

1. Introduction

The potential of SAR interferometry has motivated many scientists to apply this technique for the detection of co-seismic ground deformation signals (Wright et al., 1999; Peltzer et al., 2001; Liu et al., 2004; Parcharidis et al., 2005). However, co-seismic differential interferograms, spanning different periods after the main seismic event, may contain variable information regarding the evolution of post-seismic displacement field (Peltzer et al., 1998; Peltzer and Crampé, 1999; Donnellan et al., 2002). Such analysis was performed in the present study to investigate the spatial and temporal evolution of the post-seismic ground deformation of September 07, 1999 Athens earthquake M_w=6.0.

The main seismic event was located south of Mount Parnitha at the Thriassion Basin (Fig. 1), about 20 km west of the metropolitan area of Athens (Papadimitriou et al., 2002). The earthquake caused considerable damages in buildings and loss of many human lives (Lekkas, 2001; Fountoulis, 2004). The large number of aftershocks followed were recorded by a local digital seismograph network installed in and around the epicenter area, and operated for a period of three months (Voulgaris et al., 2000; Voulgaris et al., 2001), offering thus the opportunity for a combined assessment between DInSAR imaging and seismological data.

Earlier studies using SAR interferometry were mainly focused on the estimation of the rupture parameters by inversion of either single differential interferograms (Kontoes et al., 2000) or using stacking results in the dislocation modelling (Elias et al., 2003). Changes in the pattern of the displacement field have also been reported (Parcharidis and Foumelis, 2005). The present detailed examination of the DInSAR results aims to improve our knowledge on the evolution of the Athens 1999 post-seismic displacement field, as well as its tectonic implications.

2. Seismological data

The broader area of Athens generally thought to be characterized by low seismic activity, since no major earthquakes had been reported in the past, neither by historical catalogues nor during the instrumental period.

The epicenter location of the main shock, as reported by different seismological institutes, varied significantly. It is worth mentioning the proximity of the epicenter reported by Papadimitriou et al. (2002) to the area of maximum ground deformation detected by DInSAR.

After the main event, a large number of aftershocks were recorded reaching a total number of 3261 events. However, the rate of that seismic activity decreased exponentially after the main shock.

According to Voulgaris (2004) clustered aftershock activity near the epicenter of the main shock is observed, while a second area of high aftershock activity is located further to the East. In this area, which also represents the easternmost boundary of aftershock activity, the epicenter distribution is more diffused, and is characterized by the

* Corresponding author.
E-mail addresses: mfoum@geol.uoa.gr (M. Foumelis), parchar@hua.gr (I. Parcharidis), lagios@geol.uoa.gr (E. Lagios), voulgaris@geol.uoa.gr (N. Voulgaris).

0926-9851/$ – see front matter © 2009 Elsevier B.V. All rights reserved.
doi:10.1016/j.jappgeo.2009.02.007

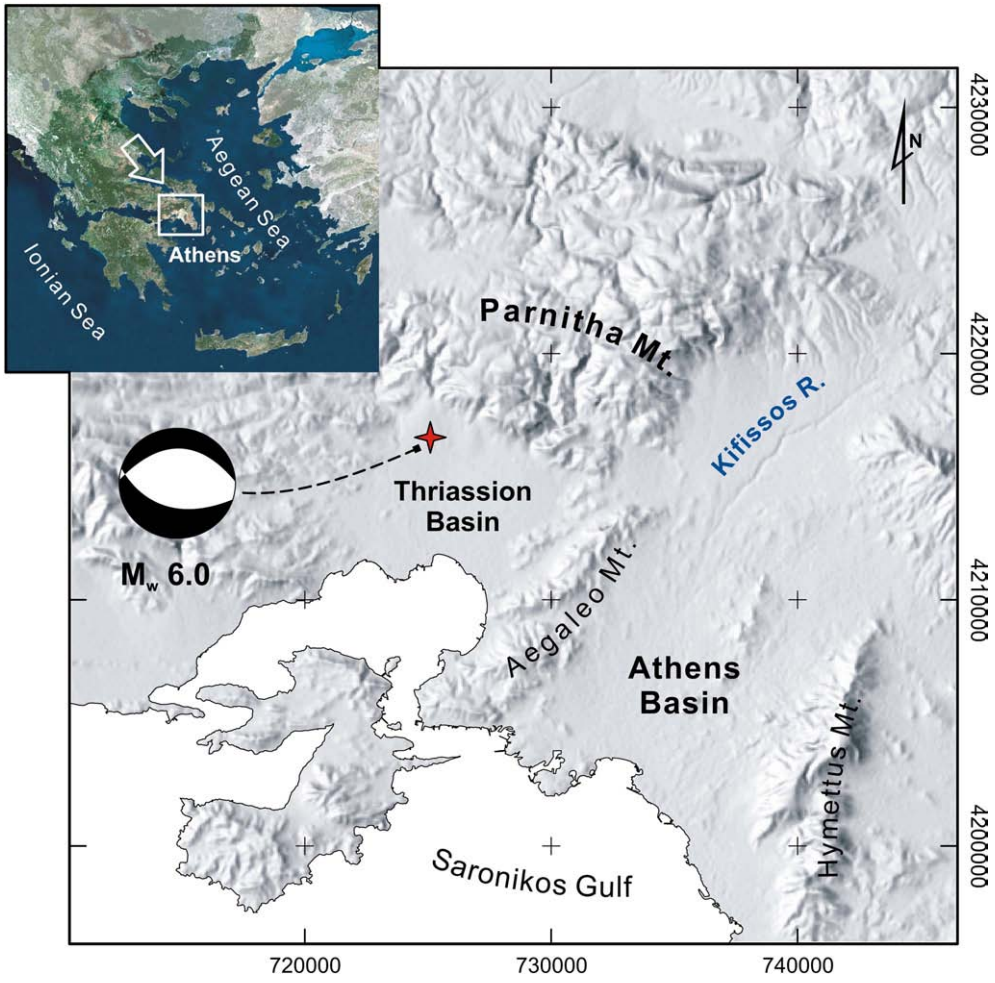

Fig. 1. Location map of the study area. Epicenter location (star) and focal mechanism of the Athens 1999 earthquake from Papadimitriou et al. (2002).

presence of a larger number of aftershocks at shallower depths and relatively larger magnitudes (Voulgaris et al., 2001; Pirli, 2002). Moreover, the highest level of seismic energy was not released in the area where the main shock was located, but at the eastern margin of the Thriassion Basin where the mountains of Parnitha and Aegaleo converge.

3. Interferometric processing

Starting from a set of C-band ERS SAR Single Look Complex (SLC) VV-polarization scenes of a descending mode (Table 1), four co-seismic differential interferograms were generated (Figs. 2 and 3). The interferograms cover the period from September to December of 1999, spanning 16, 32, 67 and 102 days after the occurrence of the main shock. The interferometric pairs are shown in Table 2, where perpendicular baseline (Bp), altitude of ambiguity (ha) and time interval (dt) values for each pair are outlined. The initial orbital state vectors for the ERS images have been taken from the Delft Institute (NL) for Earth-Oriented Space Research (DEOS) (Scharoo and Visser, 1998). The interferometric processing was performed using GAMMA s/w packages (Wegmüller et al., 1998).

During co-registration, offsets between SLC images were estimated based on the intensity cross-correlation technique. The achieved accuracy reaches a sub-pixel level. A Digital Elevation Model (DEM) of 20 m spatial resolution and height accuracy of about ±10 m was generated for the removal of the topography-related phase by digitizing 1:50,000 scale topographic maps of the Hellenic Military Geographical Service (HMGS).

Residual flat-Earth phase can be removed by correcting the slave orbital state vector or by removing phase trends in the interferograms. In this case, a non-linear least-squares estimation based on ground control points was used to determine precise interferometric baseline parameter values. After the refinement of the baselines, phase-ramps (orbital fringes) were absent from the interferograms.

The broader area of Athens is surrounded by mountains, posing thus a serious issue when dealing with topographic phase removal. However, a selection of interferometric pairs with small perpendicular baselines minimized possible topographic residuals. In addition, as the altitude of ambiguity for the selected interferometric pairs ranges between 70 m and 310 m, potential resulting topographic artefacts lie between 4 mm (0.14 phase cycles) and 0.9 mm (0.03 phase cycles) respectively, considering the given height accuracy of the DEM. Residual topographic phases were only

Table 1
List of ERS SAR scenes selected for this study

	Date	Orbit	Satellite	Track	Frame
1	1998/09/19	17854	ERS-2	465	2835
2	1999/06/26	21862	ERS-2	465	2835
3	1999/07/15	22134	ERS-2	236	2835
4	1999/09/23	23136	ERS-2	236	2835
5	1999/10/09	23365	ERS-2	465	2835
6	1999/11/13	23866	ERS-2	465	2835
7	1999/12/18	24367	ERS-2	465	2835

Please cite this article as: Foumelis, M., et al., Evolution of post-seismic ground deformation of the Athens 1999 earthquake observed by SAR interferometry, Journal of Applied Geophysics (2009), doi:10.1016/j.jappgeo.2009.02.007

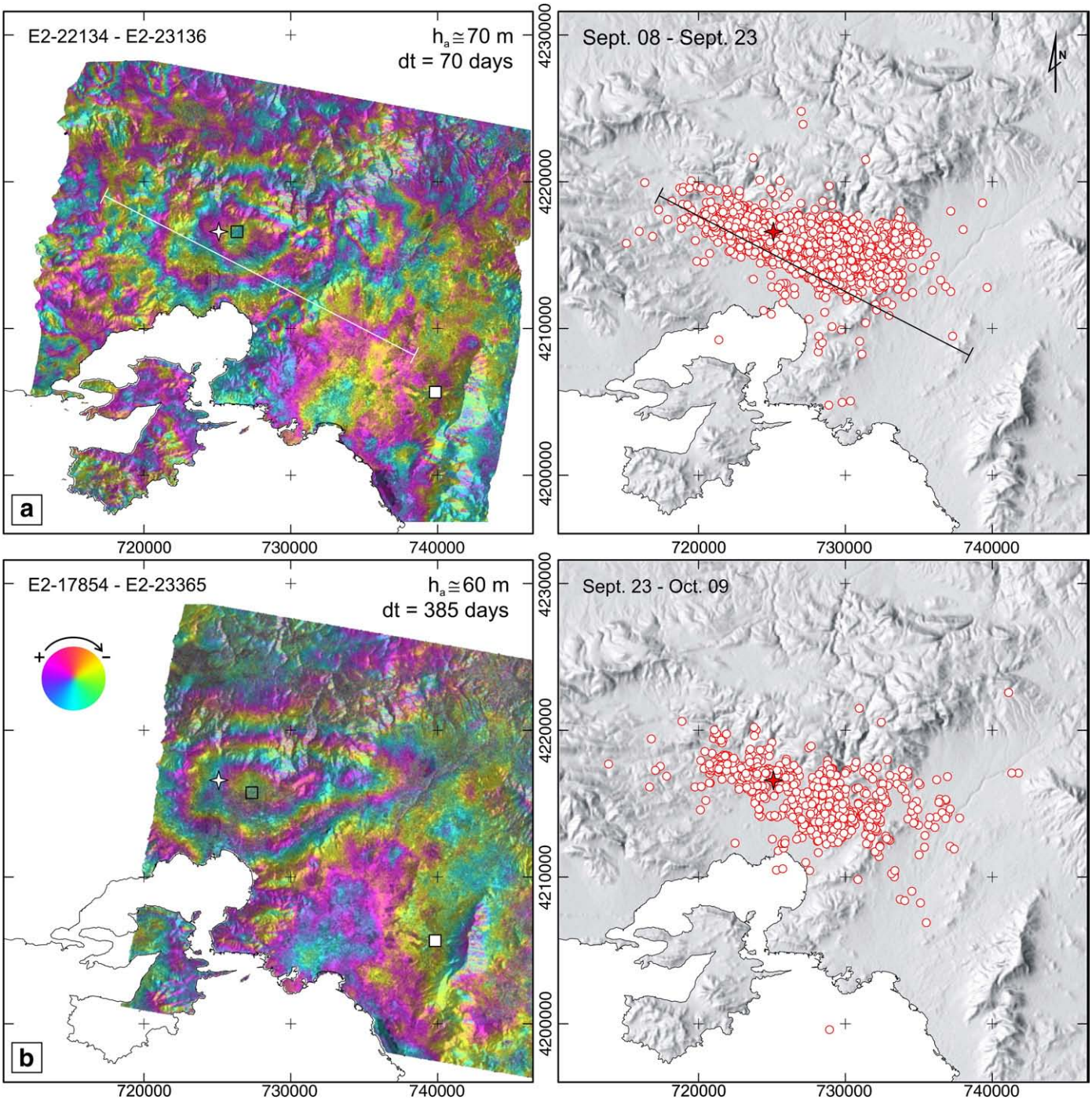

Fig. 2. Terrain corrected geocoded co-seismic differential interferograms of the Athens 1999 earthquake (left), July 1999–Sept. 1999 (a) and Sept. 1998–Oct. 1999 (b). Interferograms are displayed using one colour cycle per 28 mm of LOS deformation. Deformation pattern corresponds to ground subsidence. Spatial distribution of aftershocks for the periods between SAR acquisitions (right). The locations of the detected maximum ground deformation (transparent square) and epicenter of the Athens 1999 earthquake (star) are shown. White square corresponds to the selected DInSAR reference point.

recognized in the area of the highest elevation, at the northern part of Mount Parnitha. The former has a result to rather disrupt the continuation of fringes to the north in some differential interferograms (Fig. 3).

Local atmospheric signals could be recognized due to their temporally decorrelated nature, but not easily compensated for. Such contribution is recognized in two interferometric pairs having in common the June 26, 1999 scene (Table 2). However, it seems that atmospheric banding is constrained within the Athens Basin and affects only the easternmost extent of the deformation field examined (Fig. 3). Atmospheric phases of large wavelengths should have been removed during baseline refinement procedure.

To remove random phase offsets from the differential interferograms, we rely on the *a priori* knowledge of the deformation regime in the investigated area (Parcharidis et al., 2006) as well as on the reported intensity distribution of the earthquake (Lekkas, 2001). After identifying a reference area which is considered to be relatively stable, the differential interferograms were calibrated by forcing the phase within the selected reference area to be equal to zero for each interferogram.

Please cite this article as: Foumelis, M., et al., Evolution of post-seismic ground deformation of the Athens 1999 earthquake observed by SAR interferometry, Journal of Applied Geophysics (2009), doi:10.1016/j.jappgeo.2009.02.007

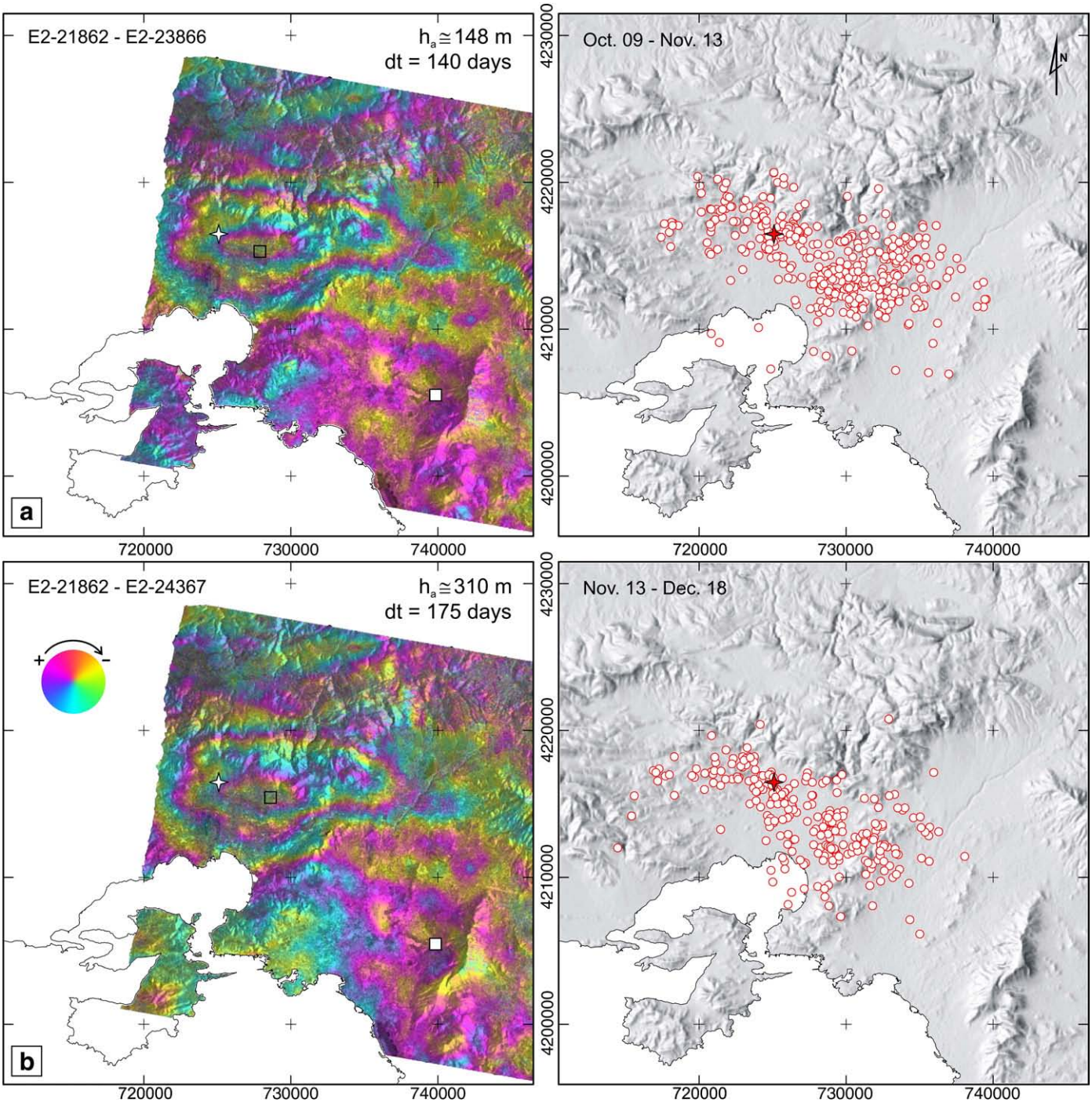

Fig. 3. Terrain corrected geocoded co-seismic differential interferograms of the Athens 1999 earthquake (left), June 1999–Nov. 1999 (a) and June 1999–Dec. 1999 (b). Spatial distribution of aftershocks for the periods between SAR acquisitions (right). The location of the spatial profile presented in Fig. 5 is also shown. White square corresponds to the selected DInSAR reference point.

The next task involves in applying an appropriate unwrapping procedure. A filtering of the differential interferograms based on the local fringe spectrum was performed using the adaptive filtering algorithm proposed by Goldstein and Werner (1998) to assist in the unwrapping by reducing phase-noise and the number of residues. Two unwrapping algorithms were tested, the Region Growing algorithm and the Minimum Cost Flow (MCF) algorithm with triangulation. Although comparable results were obtained over relatively flat areas, the MCF algorithm performed better in terms of residues and number of correctly unwrapped pixels in areas of high relief. The finally unwrapped differential interferometric phases were then converted, along the slant range, to produce the ground deformation maps.

Table 2
Interferometric parameters of the DInSAR pairs

Dates	Bp (m)	ha (m)	dt (days)
July 1999–Sept. 1999	133.7	70	70
Sept.1998–Oct. 1999	−157.3	60	385
June 1999–Nov. 1999	63.8	148	140
June 1999–Dec. 1999	−30.3	310	175

A transformation between the coordinates of the SAR imaging system (range-Doppler coordinates) and the ortho-normal map

Please cite this article as: Foumelis, M., et al., Evolution of post-seismic ground deformation of the Athens 1999 earthquake observed by SAR interferometry, Journal of Applied Geophysics (2009), doi:10.1016/j.jappgeo.2009.02.007

coordinates (in this case UTM) was performed taking into account the DEM to generate terrain corrected geocoded results (Wegmüller et al., 1998).

In order to support further analysis of the calculated ground displacements, the geocoded DInSAR data were introduced in a GIS system, together with the recorded aftershock sequence and other auxiliary data.

4. Results

The recognized deformation pattern in the generated co-seismic differential interferograms corresponds to ground subsidence (Figs. 2 and 3). The spatial distribution of the WNW–ESE trending aftershock sequence is comparable to the pattern of co-seismic ground deformation determined by the DInSAR results. The majority of the aftershock epicenters appear to be constrained within the deformed area, as it is expressed by the outer 28 mm-fringe of the interferogram of the shortest time span from the main shock (Fig. 2a).

The relation between DInSAR deformation and post-seismic activity is more evident when carefully examining the changes in the shape of the deformation fringes among the generated differential interferograms. The DInSAR pair (Fig. 2a) with the shortest temporal separation (dt=70 days), clearly shows two separate deformation centers of approximately circular shape, one over the main shock epicenter area, and another further to the east with a smaller spatial extent. As the seismic sequence evolves, these two initial deformation centers merge into one as a result of the expansion of the observed displacement field. The pattern of the displacement field gradually obtains an elliptical shape (Figs. 2b and 3) with its long axis almost parallel to the orientation of the distribution of the aftershocks. These observations are in agreement with the spatial distribution of aftershocks, where two main clusters were recognized in the same location with the DInSAR deformation centers in the early phase of the seismic sequence (Voulgaris, 2004).

For a more detailed investigation, deformation fringes were extracted from each interferogram with an interval of 14 mm using a contouring procedure. Spline filtering of the generated vector data was applied to smooth small-scale oscillations of the fringes. Both spatial and temporal evolution of the post-seismic displacement field as deduced by the differential interferograms is better represented when fringes of equal displacement are separated from each interferogram and then overlapped (Fig. 4). A propagation of ground deformation during the post-seismic period to the east of the main shock location, towards the metropolitan area of Athens, is evident. Moreover, the progressive expansion of the displacement filed from two separate centers is also clearly shown.

In order to better characterize the displacement field a WNW–ESE spatial profile (Fig. 2a) is presented, showing the range of observed LOS displacements and the total moment release of the aftershocks during the time intervals of the DInSAR measurements (Fig. 5). The range of LOS displacements for each DinSAR period was calculated by the superimposition of several parallel profiles covering the entire displacement field. Three dimensional aftershocks locations were perpendicularly projected on the selected profile plane. The calculation of the seismic moment of the aftershocks from the estimated duration magnitudes was performed using the empirical equations given in Pirli (2002). Considering possible errors in the aftershocks locations as well as the temporal separation of the aftershocks occurrence, only a qualitative rather than a robust correlation between aftershocks total moment release and DInSAR displacements could be achieved. Nevertheless, a correspondence particularly in the early phase of the seismic sequence (two deformation centers) could be recognized. The slight deviation between the moment release centers and ground displacement maxima is due to the effect of the projection of the aftershocks on the profile. The increase of the range displacements and the gradual migration along the SE direction is also better visualized (Fig. 5a).

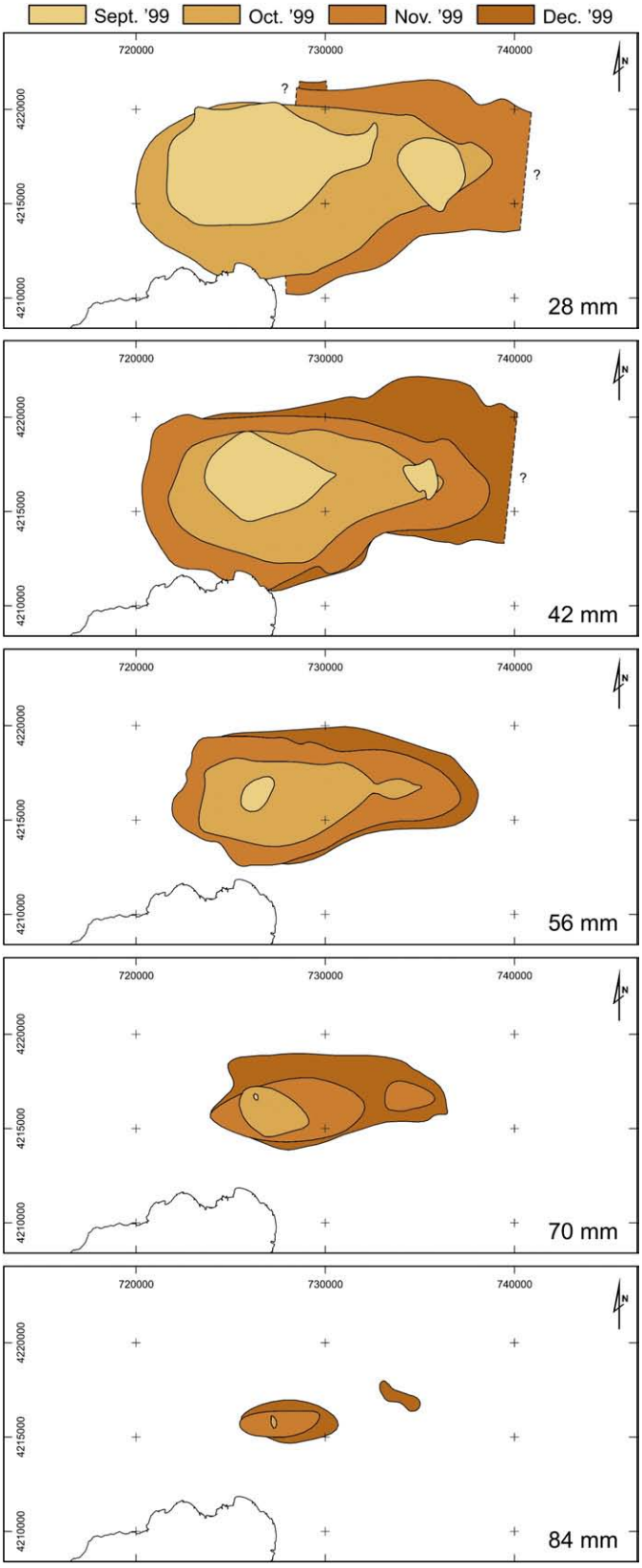

Fig. 4. Evolution of the post-seismic displacement field of the Athens 1999 earthquake. Deformation fringes of equal values were extracted from each interferogram and then overlapped to show how ground deformation evolves.

Please cite this article as: Foumelis, M., et al., Evolution of post-seismic ground deformation of the Athens 1999 earthquake observed by SAR interferometry, Journal of Applied Geophysics (2009), doi:10.1016/j.jappgeo.2009.02.007

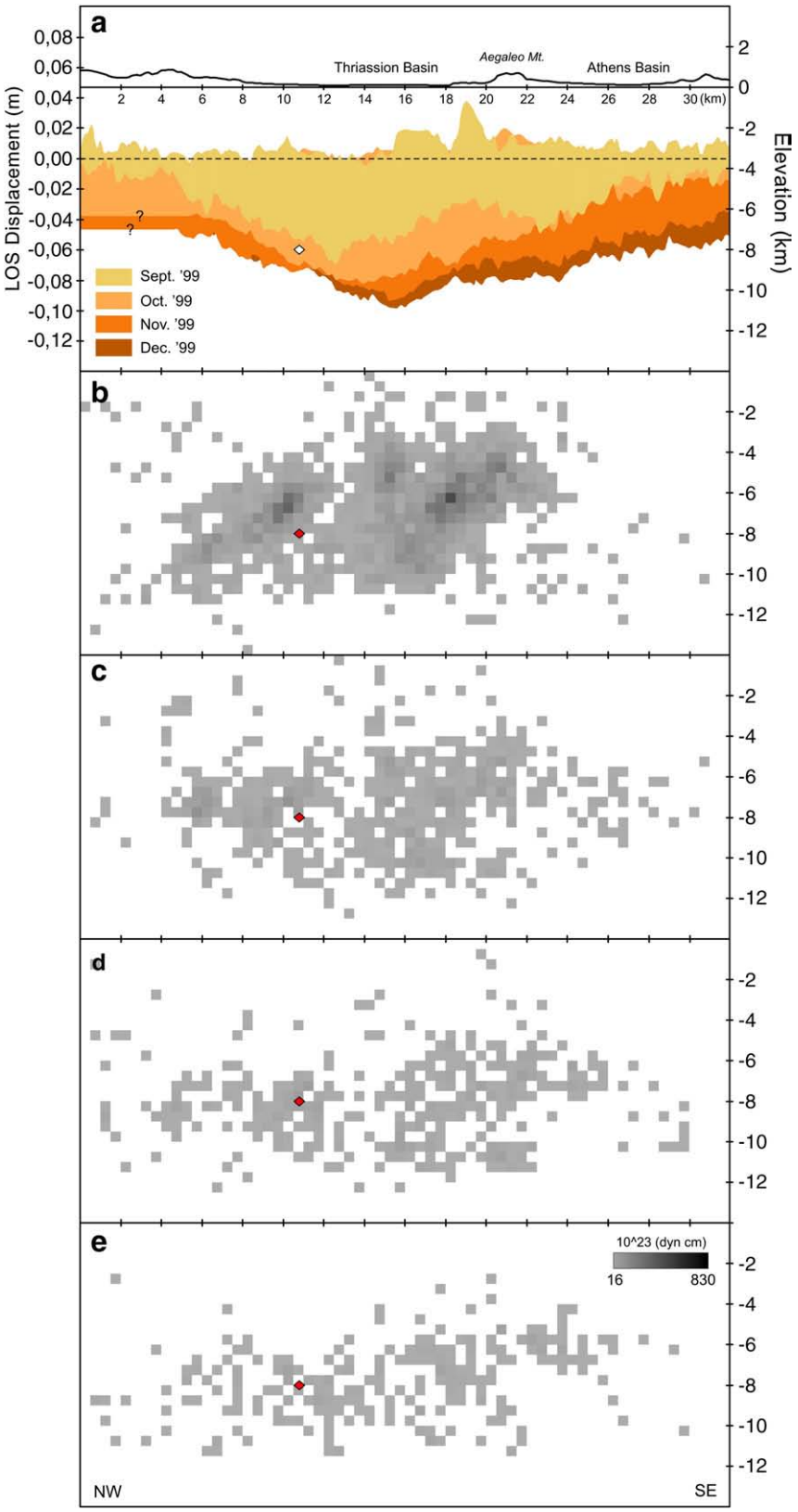

Fig. 5. Spatial profile showing the range of LOS displacement (a) for the different DInSAR periods and the corresponding total seismic moment release of the aftershocks, till Sept. 23 (b), Sept. 23–Oct. 10 (c), Oct. 10–Nov. 13 (d) and Nov. 13–Dec. 18 (e). The location of the profile is shown in Fig. 2a. Negative LOS displacement values correspond to ground subsidence (increase of slant range distance). The question marks indicate the limited extend of the differential interferograms to the NW of the displacement field. The hypocenter of the main shock as calculated by Papadimitriou et al. (2002) is also shown (diamond).

Similar remarks are drawn when examining the evolution in space of the detected maximum ground deformation of each interferometric period considered. Distances between deformation maxima and main shock epicenter tend to increase and migrate toward an almost SE direction as the seismic sequence evolves (Fig. 6). Meanwhile, the exponential decrease of the observed

Please cite this article as: Foumelis, M., et al., Evolution of post-seismic ground deformation of the Athens 1999 earthquake observed by SAR interferometry, Journal of Applied Geophysics (2009), doi:10.1016/j.jappgeo.2009.02.007

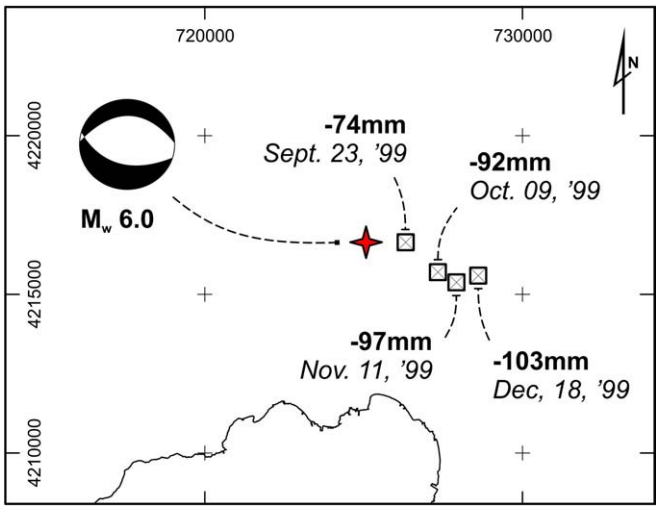

Fig. 6. Spatial evolution of the ground deformation maxima (squares) during the post-seismic period of the Athens 1999 earthquake (star).

magnitude of ground deformation over time (Fig. 7) is in accordance with the decrease of rate of seismic activity.

The fact that such systematic changes in the magnitude and the location of the deformation maxima exist, underlines the contribution of post-seismic deformation, regardless of its relatively small magnitude scales, to the cumulative ground deformation observed by SAR interferometry. Differences in maximum ground deformation values between the co-seismic DInSAR pairs with the shortest (July 1999–Sept. 1999, 16 days) and longest (June 1999–Dec. 1999, 102 days) temporal separation from the main shock are 29 mm and 12 mm for the uncalibrated and calibrated differential interferograms, respectively. These values correspond to the indirect measurement of part of the total post-seismic ground deformation, as a considerable amount of post-seismic deformation is included even in the co-seismic interferogram of the shortest temporal span (Fig. 2a). Such magnitudes of ground deformation are within the theoretical minimum threshold of the conventional DInSAR technique (roughly half of the wavelength = 28 mm).

It is important to notice that any attempts to measure directly the post-seismic deformation simply using post-seismic interferometric pairs were not succeeded, mainly due to geometrical limitations such as the perpendicular baseline and to a lesser extend to temporal decorrelation.

5. Discussion

A general remark that should be made regarding the generated differential interferograms concerns the spatial continuity of the displacement field. The above observation implies that the rupture did not reach the surface. No trace of the seismic fault was also identified by field geological campaigns (Mariolakos and Fountoulis, 2000a, 2000b). The spatial distribution of secondary geodynamic phenomena (fractures, rockfalls, landslides etc.) all over the mountainous area of Parnitha supports this hypothesis. Furthermore, the depth distribution of the well-located aftershocks (RMS < 0.1 s and ERH, ERZ < 1 km) ranges between 3 km and 10 km with very few aftershocks located at shallower depths (Voulgaris et al., 2001).

Both seismological and DInSAR observations support the hypothesis that the rupture was initiated at the western edge of the seismic fault plane, while most of the seismic moment release was distributed east of the main shock epicentral area.

Any changes in the observed magnitude of deformation for the period following the main event, especially during the evolution of the seismic sequence, should rather be attributed to post-seismic deformation phenomena. This is evident as all the generated differential interferograms contain the deformation resulted from the main event of the Athens 1999 seismic sequence. An assumption however is made that other sources of deformation prior to the earthquake for the time interval sampled by the selected SAR acquisitions or during the post-seismic period, should not exist or should be below the detectable range by conventional DInSAR technique. The validity of this assumption can be controlled as ground deformation rate in the area is low (few millimeters per year) (Parcharidis et al., 2006) and just one interferometric pair (Sept. 1998–Oct. 1999) has large temporal separation (385 days) extending about a year before the earthquake.

The detected differences of ground deformation of the co-seismic DInSAR pairs could generally be attributed, apart from other deformation sources, to the cumulative energy release by the aftershock sequence. Particularly, the intensive clustered aftershock activity to the east, attributed to the re-activation of a secondary rupture zone (Kontoes et al., 2000), could possibly be related to the evolution of the observed surface displacement field. The distance between successive deformation maxima ranges from 0.8 km to 1.8 km, in an area where the entire displacement field does not exceed 25 km along the E–W direction. The propagation to the SE of the ground deformation maxima as the seismic sequence evolves is in agreement with rupture directivity phenomena mentioned in various seismological studies (Roumelioti et al., 2003; Baumont et al., 2004; Roumelioti et al., 2004).

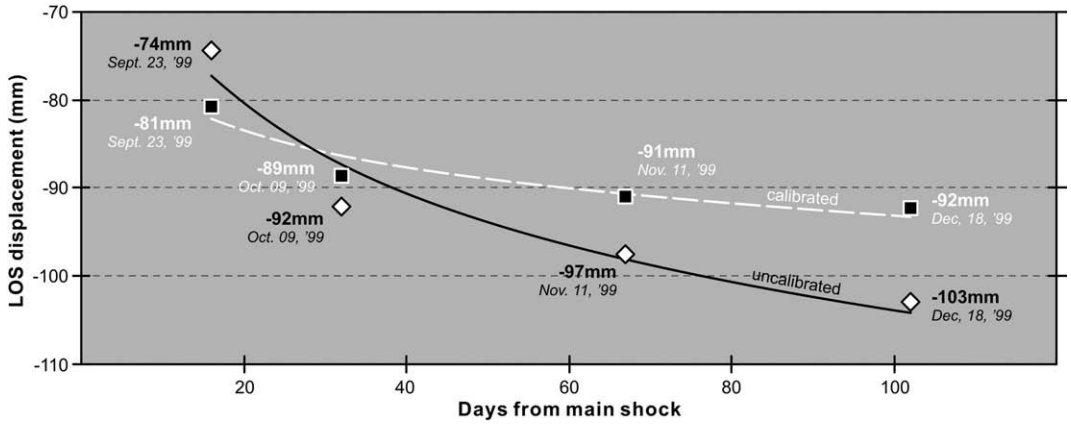

Fig. 7. Temporal evolution of maximum ground deformation, before and after the calibration of the differential interferograms. Negative LOS displacement values correspond to ground subsidence (increase of slant range distance).

Please cite this article as: Foumelis, M., et al., Evolution of post-seismic ground deformation of the Athens 1999 earthquake observed by SAR interferometry, Journal of Applied Geophysics (2009), doi:10.1016/j.jappgeo.2009.02.007

It was shown in various studies that aseismic afterslip on the main rupture zone, as well as poro-elastic rebound in the shallow crust, could have more significant contribution to post-seismic ground deformation following a seismic event than cumulative aftershocks (Peltzer et al., 1998; Donnellan et al., 2002). The driving mechanisms of post-seismic deformation in the present study, however, cannot fully be resolved simply by using DInSAR measurement and further investigation on this matter is required.

It is important to notice that the co-seismic interferogram with the shortest temporal separation from the main shock (July 1999–Sept. 1999, 16 days) still contains large amount of post-seismic related deformation, not allowing the calculation of the ground deformation produced only by the main seismic event. The use of such interferograms in dislocation modelling without accounting for the post-seismic deformation will lead to the overestimation of parameters such as the size of the rupture zone and the amplitude of the co-seismic slip. Similarly, averaging different co-seismic interferograms by means of stacking in order to reduce the atmospheric contributions from the deformation signals will result to similar overestimations. Such kind of overestimations of source parameters determined by space geodetic techniques are already mentioned in the literature, when compared to seismological calculations (Wright et al., 1999; Kontoes et al., 2000).

Acknowledgements

The present study was carried out within the framework of ESA's Category-1 Project (ID: 3333), where provision of ERS SAR imagery is acknowledged. It was financed by the European Union (75%), the General Secretariat for Research & Technology of the Ministry of Development of the Hellenic Republic (25%), and the Private Sector TerraMentor EOOS, within the framework of action 8.3 of the EU "Competitiveness" — 3rd Community Support Programme.

References

Baumont, D., Scotti, O., Courboulex, F., Melis, N., 2004. Complex kinematic rupture of the Mw 5.9, 1999 Athens earthquake as revealed by the joint inversion of regional seismological and SAR data. Geophysical Journal International 158, 1078–1087.

Donnellan, A., Parker, Peltzer, G., 2002. Combined GPS and InSAR models of postseismic deformation from the Northridge earthquake. Pure and Applied Geophysics 159, 2261–2270.

Elias, P., Sykioti, O., Kontoes, C., Avallone, A., Van Gorp, S., Briole, P., Paradissis, D., 2003. Development of a procedure for correcting and reducing unwrapping artefacts using a set of ERS SAR interferograms. Case of the September 7, 1999 Athens Earthquake. Proceedings of Fringe '03 Workshop, Frascati, Italy.

Fountoulis, I., 2004. The neotectonic macrostructures and the geological basement, the main factors controlling the spatial distribution of the damage and geodynamic phenomena resulting from the Kalamata (13 September 1986) and Athens (7 September 1999) earthquakes. In: Lekkas, E.L. (Ed.), Earthquake Geodynamics: Seismic Case Studies. WIT Press.

Goldstein, R., Werner, C., 1998. Radar interferogram filtering for geophysical applications. Geophysical Research Letters 25 (21), 4035–4038.

Kontoes, C., Briole, P., Sachpazi, M., Veis, G., Elias, P., Sykioti, O., Remy, D., Kotsis, I., 2000. Displacement field and fault model for the September 7, 1999 Athens earthquake inferred from ERS2 satellite radar Interferometry. Geophysical Research Letters 27 (24), 3989–3992.

Lekkas, E., 2001. The Athens earthquake (7 September 1999): intensity distribution and controlling factors. Engineering Geology 59, 297–311.

Liu, G.X., Ding, X.L., Li, Z.L., Li, Z.W., Chen, Y.Q., Yu, S.B., 2004. Pre- and co-seismic ground deformations of the 1999 Chi-Chi, Taiwan earthquake, measured with SAR interferometry. Computers & Geosciences 30, 333–343.

Mariolakos, I., Fountoulis, I., 2000b. The Athens earthquake September 7, 1999 neotectonic regime and geodynamic phenomena. Annales Geologiques des Pays Helliniques 38 (B), 165–174.

Papadimitriou, P., Voulgaris, N., Kassaras, I., Kaviris, G., Delibassis, N., Makropoulos, K., 2002. The Mw=6.0, 7 September 1999 Athens earthquake. Natural Hazards 27 (1), 15–33.

Parcharidis, Is., Foumelis, M., 2005. On the assessment of co-seismic InSAR images of different time span associated to Athens (Greece) 1999 earthquake. Proceedings of IGARSS '05 7, pp. 5251–5254.

Parcharidis, Is., Zaré, M., Foumelis, M., Lagios, E., 2005. Seismotectonic investigation on the BAM earthquake prone area (Iran) based on ASAR interferometry. Proceedings of RAST '05, pp. 673–677.

Parcharidis, Is., Lagios, E., Sakkas, V., Raucoules, D., Feurer, D., Le Mouelic, S., King, C., Carnec, C., Novali, F., Ferretti, A., Capes, R., Cooksley, G., 2006. Subsidence monitoring within the Athens Basin (Greece) using space radar interferometric techniques. Earth, Planets and Space Journal 58, 505–513.

Peltzer, G., Crampé, F., 1999. Evidence of non-linear elasticity of the crust from the Mw7.6 Manyi (Tibet) earthquake surface displacement field. Science 286 (5438), 272–276.

Peltzer, G., Rosen, P., Rogez, F., 1998. Poro-elastic rebound along the Landers 1992 earthquake surface rupture. Journal of Geophysical Research B: Solid Earth 103 (B12), 30131–30145.

Peltzer, G., Crampe, F., Rosen, P., 2001. The Mw 7.1, Hector Mine, California earthquake: surface rupture, surface displacement field, and fault slip solution from ERS SAR data. Comptes Rendus de l'Academie des Sciences A 333 (9), 545–555.

Pirli, M., 2002. Seismic characteristics of the aftershock sequence of Athens earthquake (07/09/1999, Ms=5.9). Master Thesis, National & Kapodistrian University of Athens, Department of Geophysics — Geothermics, p.237, (in Greek).

Roumelioti, Z., Kiratzi, A., Theodulidis, N., Kalogeras, I., Stavrakakis, G., 2003. Rupture directivity during the September 7, 1999 (Mw5.9) Athens (Greece) earthquake inferred from forward modelling of strong ground motion. Pure and Applied Geophysics 160, 2301–2318.

Roumelioti, Z., Kiratzi, A., Theodulidis, N., 2004. Stochastic strong ground-motion simulation of the 7 September 1999 Athens (Greece) earthquake. Bulletin of the Seismological Society of America 94 (3), 1036–1052.

Scharoo, R., Visser, P., 1998. Precise orbit determination and gravity field improvement for the ERS satellites. Journal of Geophysical Research 103, 8113–8127.

Voulgaris, N., 2004. Contribution of GIS to analysis of the 7 September 1999 Athens earthquake. In: Lekkas, E.L. (Ed.), Earthquake Geodynamics: Seismic Case Studies. WIT Press.

Voulgaris, N., Kassaras, I., Papadimitriou, P., Delibassis, N., 2000. The September 7, 1999 Athens earthquake sequence recorded by Cornet network: preliminary results of source parameters determination of the main shock. Annales Geologiques des Pays Helliniques 38 (B), 29–39.

Voulgaris, N., Pirli, M., Papadimitriou, P., Kassaras, I., Makropoulos, K., 2001. Seismotectonic characteristics of the area of western Attica derived from the study of the September 7, 1999 Athens earthquake aftershock sequence. Bulletin of the Geological Society of Greece 34 (4), 1645–1651.

Wegmüller, U., Werner, C., Strozzi, T., 1998. SAR interferometric and SAR differential interferometric processing chain. Proceedings of IGARSS '98 2, 1106–1108.

Wright, T.J., Parsons, B.E., Jackson, J.A., Haynes, M., Fielding, E.J., England, P.C., Clarke, P.J., 1999. Source parameters of the 1 October 1995 Dinar (Turkey) earthquake from SAR interferometry and seismic body wave modelling. Earth and Planetary Science Letters 172 (1–2), 23–37.

Please cite this article as: Foumelis, M., et al., Evolution of post-seismic ground deformation of the Athens 1999 earthquake observed by SAR interferometry, Journal of Applied Geophysics (2009), doi:10.1016/j.jappgeo.2009.02.007